PUBLICATION

MUSTANG

A MUltiple Space and Time scale Approach for the quaNtification of deep saline formations for CO_2 storaGe

Project Number:227286

AUTHORS: *Fritjof Fagerlund, Auli Niemi, Jacob Bensabat, Vladimir Shtivelman*

TITLE: *Design of a two-well field test to determine in situ residual and dissolution trapping of CO_2 applied to the Heletz CO_2 injection site*

The research leading to these results has received funding from the European Community's Seventh Framework Programme [FP7/2007/2013) under grant agreement n° [227286]

Status	AUTHOR VERSION
Date	2013
Publisher	Science Direct
Reference	International Journal of Greenhouse Gas Control, Vol. 19, pp. 642–651

Design of a two-well field test to determine in-situ residual and dissolution trapping of CO_2 applied to the Heletz CO_2 injection site

Fritjof Fagerlund[a*], Auli Niemi[a], Jacob Bensabat[b] Vladimir Shtivelman[c]

a) Uppsala University, Earth Sciences, Uppsala, Sweden
b) Environmental & Water Resources Engineering Ltd, Haifa, Israel
c) Geophysical Institute of Israel, Lod, Israel
* Corresponding author. Address: Uppsala University, Department of Earth Sciences, Villavagen 16, 75236 Uppsala, Sweden. Tel. +46 18 471 7166. Fax. +46 18 551124. E-mail: fritjof.fagerlund@geo.uu.se

Abstract
Field testing is a critical step to improve our knowledge on in situ-trapping mechanisms of CO_2 injected in geological formations and their relative importance. In this study, we present a two-well test sequence aimed at quantifying field values of both residual and dissolution trapping of CO_2. Then, we apply it to the Heletz experimental CO_2 injection site, using numerical modelling. The sequence includes a hydraulic test to measure residual $scCO_2$ saturation and a novel tracer technique, together with measurements of abstracted fluid compositions for quantification of the rate of CO_2 dissolution in the reservoir. The proposed tracer technique uses a tracer with negligible aqueous solubility, which is injected with the $scCO_2$ and enriched in the $scCO_2$ phase as CO_2 dissolves. We show that this tracer can provide direct information about the dissolution of mobile $scCO_2$. We also show that the rate of abstracted dissolved CO_2 can be used to predict the total rate of CO_2 dissolution, provided that the amount of dissolved CO_2 in the formation stabilizes, and that this can be achieved with the proposed abstraction scheme. We conclude that the combination of these measurements is a promising tool for detailed field-scale characterization of residual and dissolution trapping processes.

Keywords: CO_2, geological storage, dissolution, residual trapping, field experiment

1. Introduction
Carbon dioxide capture and storage (CCS) is a potential key technology, in the global effort of mitigating the impact of greenhouse gas emissions to the atmosphere. However, successful implementation of CO_2 geological storage projects requires that secure storage at the proposed field sites can be demonstrated. CO_2 trapping by different processes improves the storage security and are critical for the fate of the injected CO_2 as well as storage security and reservoir capacity in many geological settings under consideration for CO_2 geological storage. Highly-controlled scientific CO_2 injection experiments at the field scale are critical both for the demonstration of CCS technology and to improve current knowledge about CO_2 trapping processes at field scale, under the actual conditions of typical storage sites.

Due to the temperature field prevailing in the candidate storage layers, geologically stored CO_2 remains buoyant in brine even at depths where it has been compressed to a dense supercritical state (>800 m) and tends to migrate upwards by buoyancy unless it is trapped by other processes. The main general trapping mechanisms are (i) structural and stratigraphic trapping, (ii) residual phase trapping, (iii) dissolution trapping and (iv) mineral trapping (IPCC, 2005). A structural trap in the form of a low-permeability cap rock layer overlying the target formation for storage is generally a prerequisite for taking a site into consideration for CO_2 geological storage. While mineral trapping typically becomes significant only after long

times (order of 1000s of years), residual phase and dissolution trapping can contribute to increased storage security already from the end of the CO_2 injection phase. CO_2 geological storage techniques primarily relying on these trapping mechanisms have also been proposed (e.g. Qi et al., 2009; Suekane et al., 2008), for example in open, mildly dipping formations, which lack a true structural trap (Akervoll et al., 2006).

Laboratory studies have investigated fluid migration and residual phase trapping in supercritical CO_2 ($scCO_2$) – brine systems at the core scale (e.g. Krevor et al., 2011) and in analogous two-phase systems at the bench scale (e.g. Fagerlund et al., 2007a, b; Polak et al., 2010). CO_2 dissolution and convective mixing has been investigated experimentally (Kneafsy and Pruess, 2010; Neufeld et al. 2010) as well as by theoretical analyses (e.g. Riaz at al., 2006). Several modelling studies have also been conducted to further study both residual phase trapping and dissolution trapping (e.g. Hesse et al., 2009, Pau et al., 2010).

Well-controlled field experiments investigating residual phase and dissolution trapping in-situ, under influence of geological heterogeneity, however, remain scarce. Yet, field testing is critical to improve understanding of how the CO_2 trapping will take place in-situ and to assess the relative importance of the different trapping mechanisms at field sites for geological storage. Given the challenge to measure fluid flow and trapping processes in kilometre-deep reservoirs with few boreholes and limited knowledge of the spatial distribution of geological parameters, the design of field tests that can accurately quantify the CO_2 trapping is also challenging. At the Frio site, Texas, a small-scale CO_2-injection was passively monitored at a nearby up-dip well (Doughty et al., 2008) using fluid sampling, tracers, well logs and cross-hole seismics. This study demonstrated the importance of combining different measurements for better characterization and the integration of these in a flow and transport model for the field site. At the Ketzin site, Germany, CO_2 injections have been monitored from three boreholes using geophysical, hydraulic and tracer techniques (e.g. Würdemann et al., 2010). Experiences from Ketzin highlight the importance of geological heterogeneity on migration and fate of the injected CO_2 (Lengler et al., 2010).

Zhang et al. (2011) have proposed a single-well test method to measure the residual gas saturation S_{gr} (of $scCO_2$) using a combination of hydraulic, thermal and push-pull tracer tests at the Otway field site, Australia. Zhang et al. (2011) demonstrate that the hydraulic test where CO_2-saturated water is injected into the formation containing residually trapped CO_2 is highly sensitive to S_{gr} because the relative permeability to the aqueous phase is reduced in presence of residual $scCO_2$. In the thermal test the formation is heated from the borehole and then allowed to cool. The temperature in the borehole depends on the thermal conductivity, which in turn depends on the fluid saturations. Thus, it can also be used to measure S_{gr}. This test can reach a couple of metres into the formation from the borehole depending on the time and intensity of heating as well as the reservoir properties and conditions.

The retardation of a tracer in the flowing phase (e.g. water) due to partitioning into an immobile immiscible phase (e.g. gas or oil) can also be used to infer the presence and quantity of the immobile phase. This can be done both in single-well push-pull tests and two-well interwell tests. Partitioning interwell tracer tests (PITTs) have been developed and used in the petroleum industry for measurement of residual oil saturation (Du and Guan, 2005; Tang, 2005, Sinha et al., 2004). PITTs have also been used to measure non-aqueous phase liquid (NAPL) saturations in NAPL-water two-phase systems (e.g. Nelson et al., 1999; Jin et al., 1995) and the unsaturated zone (e.g. Mariner et al., 1999). However, field methods to determine dissolution of CO_2 in-situ have, to the best of our knowledge, not been presented in literature.

Within the EU-FP7 MUSTANG project, a series of field experiments are being designed for the Heletz field site, Israel (Fig. 1), where two wells to the target formation for CO_2 injection have recently been drilled and are currently being completed and instrumented. The series of experiments will include well logging, flowing-fluid electrical conductivity logging as well as hydraulic and tracer tests without CO_2 to characterize the formation prior to CO_2 injections. Then, a series of experiments involving CO_2 injections will be performed to characterize parameters and processes affecting the fate of the injected CO_2. Specifically CO_2 trapping processes will be characterized using both single-well and interwell tests.

In single-well push pull experiments, the influence of geological heterogeneity on the fluid flow and transport parameters is somewhat reduced because the fluids are pushed out and pulled back through the same flow channels. In interwell tests the processes are affected by geological heterogeneity between the wells. The combination of single-well and interwell tests has therefore been deemed effective for studying CO_2 trapping processes as well as the effect of heterogeneity on these processes. In a dipole test with active abstraction of fluids from one well, a controlled, converging flow field is established which facilitates careful monitoring of abstracted fluid composition and tracers.

In this study, a two-well dipole test sequence for quantifying both residual and dissolution trapping of CO_2 in situ is proposed. The sequence includes: (i) a hydraulic test to measure residual $scCO_2$ saturation, and (ii) a novel tracer technique together with measurements of abstracted fluid compositions for quantification of the effective rate of CO_2 dissolution in the formation. The hydraulic test will be repeated before and after CO_2 injection and the residual $scCO_2$ saturation will be inferred from differences in pressure responses. The proposed tracer technique uses a tracer with very small or, preferably, negligible aqueous solubility, which is mixed into and injected with the $scCO_2$. As the CO_2 dissolves into formation brine, the tracer will be enriched in the $scCO_2$ phase. The hypothesis therefore was that when $scCO_2$ arrives at the abstraction well, its tracer content carries direct information about how much dissolution this mobile $scCO_2$ has undergone on its way through the formation. Using numerical modelling, the proposed test sequence was applied to Heletz field site, for which such test is under planning. The two main objectives of this study were: (i) to present and demonstrate a viable two-well test sequence for the quantification of both effective residual-phase and dissolution trapping of CO_2 in situ as the CO_2 flows through the storage formation, and (ii) to test the hypothesis that an $scCO_2$-borne tracer of negligible aqueous solubility provides useful information for the quantification of in-situ CO_2 dissolution in this test configuration. Additional tests to further improve an integrated determination of the trapping parameters, such as thermal tests, can easily be added to the proposed test sequence but are not the focus of this study.

2. Methods

2.1 Concept idea and proposed test sequence for the dipole experiment

A timeline for the proposed test sequence is shown in Fig. 2, including fluid injections to the injection well (I) (upper part of Fig. 2) and withdrawal from the abstraction well (A) (lower part of Fig. 2). Abstraction of fluids at a constant rate from well A occurs continuously throughout the entire test and controls the groundwater flow field. The first part of the sequence is a reference hydraulic test with no $scCO_2$ in the formation. This is done by injecting water into the formation from well I for 1 day and measuring the pressure response in both wells (marked “a” in Fig. 2). Next, injection is stopped for 1 day (but the constant abstraction continues) and then CO_2 together with a negligible-solubility tracer (NST) is injected (marked “b” in Fig. 2). A CO_2 injection of 1000 tons at a rate of 5 tons/h will take 8.3

days to perform. After the CO_2 has been injected then injection is again stopped but abstraction continues to draw fluids to the abstraction well. Once the $scCO_2$ breaks through to well A (shown schematically in Fig. 3a), the $scCO_2$-borne NST together with the dissolved CO_2 in the aqueous phase carry information about the dissolution of CO_2 that has occurred between the wells. After a period of abstraction, the flow of $scCO_2$ to the abstraction well will cease, thus indicating that the $scCO_2$ remaining in the formation is trapped as residual phase (marked "c" in Fig. 2, and shown schematically in Fig. 3b). How long this takes (time X in Fig. 2) depends on the flow and trapping in the formation. At this time a hydraulic test using CO_2-saturated brine is performed to measure the residual trapping (marked "d" in Fig. 2). As in the reference test, water is injected for 1 day and the pressure response is monitored in both wells. CO_2-saturated brine is used to avoid any additional dissolution of CO_2 during this test.

A thermal test similar to that proposed by Zhang et al. (2011) could also be included in the test sequence and should in that case precede both the hydraulic reference test and the second hydraulic test. As seen in Fig. 2, we propose that while abstraction is continuous, injections are only performed for the hydraulic tests and the CO_2 injection. The reason is that additional brine injection would dissolve CO_2 and complicate the measurements of both residual phase and dissolution trapping. A standard PITT may also be added at the time when the $scCO_2$ is at residual saturation, but may in practice it may be difficult to perform this type of test without dissolving the residually trapped $scCO_2$.

In the field test fluid samples will be taken in a fluid sampling cylinder at the depth of the target layer. The container preserves the pressure of the sample when it is brought to the surface for analysis of fluid composition and concentrations of dissolved CO_2 and tracers. The tracer of very low aqueous solubility used in the modelling presented here is hypothetical because detailed data on partitioning behaviour for promising tracer candidates are still lacking for the $scCO_2$-brine system at reservoir temperature and pressure conditions. Judging available partitioning data for air-water systems (e.g. Wen and Muccitelli, 1979) perfluorocarbons such as C_3F_8 and C_2F_6 are promising candidates while the somewhat more soluble SF6 may also be useful. In practice, a combination of tracers with slightly different partitioning behaviour may also be applied. The tracer used in this modelling study was given a Henry's coefficient of 2.0×10^{12} Pa^{-1}, which implies a very strong affinity for the gaseous phase. For comparison, Pruess et al. (2005) report an air-water Henry's coefficients of 3.29×10^{10} Pa for SF_6, which was used in the Frio CO_2 injection experiment and Henry's coefficients of 3.86×10^9 Pa and 2.63×10^9 Pa for the noble gas partitioning tracers Kr and Xe, respectively (used at Otway, Zhang et al., 2011), all at 65°C.

2.2 Numerical codes

To test and demonstrate the proposed test sequence, a numerical model for flow and transport of CO_2, brine and tracers in the Heletz target formation was constructed. The TOUGH2 numerical code for non-isothermal multiphase flow and transport (Pruess et al., 1999) was used in combination with two different equation-of-state (EOS) modules: ECO2N (Pruess, 2005) and EOS7C (Oldenburg et al., 2004). ECO2N (Pruess, 2005) is a module developed for supercritical or gaseous CO_2, water, NaCl, and heat. It uses a state-of-the art EOS for CO_2 at reservoir conditions, handles dry out and salt precipitation due to brine evaporation into the CO_2-rich phase, and had good numerical performance (few convergence issues) applied to the simulation problems of this study. However, it lacks the capability to model tracer transport in the $scCO_2$-brine system. The EOS7C model (Oldenburg et al., 2004) handles mixtures of CO_2 and methane (CH_4), brine, water, heat and a user-defined tracer in a two-phase system. This code has the capability to model the tracer transport in the $scCO_2$-brine system of interest, but typically had numerical stability problems and would fail to converge during the later stage of

the simulated test-sequence. Therefore a combined approach using both these modules was taken. The hydraulic test and the state of the system when it was time to perform it were evaluated using the ECO2N model which could run on a high resolution grid all the way to the completion of the test sequence. The evaluation of tracer transport was done using the EOS7C module on a grid with somewhat fewer blocks than for the ECO2N model, but still enough to demonstrate the tracer behaviour in the system. Because the idea was to use measurements of tracer in the $scCO_2$ phase, the tracer transport only needed to be evaluated during the time that $scCO_2$ was abstracted.

In both modules, capillary pressure was described using the Brooks and Corey (1964) (BC) function and relative permeability was described using the Brooks and Corey (1964) – Burdine (1953) (BCB) function. Hysteresis in these constitutive relations has an effect of the final trapped $scCO_2$ saturation (S_{gr}), particularly in heterogeneous media where trapping also occurs at capillary barriers (Fagerlund et al., 2008). In such models S_{gr} depends on the previous maximum saturation $S_{gr,max}$ (e.g. Land 1968). In this study our focus was on the sensitivity of different measurements to the trapping properties rather than modelling of the trapping process itself. Therefore we chose a simplified approach where hysteresis was not accounted for and that uses a constant final trapped saturation (S_{gr}) as implemented to the TOUGH2 code by Fagerlund et al. (2008). Variation of S_{gr} allowed investigation of whether the test was sensitive to different trapped saturations. However, in the next phase, when evaluating field data, a model including hysteresis should be used.

2.3 Conceptual model

The geological model was based on the scientific CO_2-injection field site at Heletz, Israel (Fig. 1), which is part of EU-FP7 MUSTANG project. The target formation for CO_2 injection consists of a lower-cretaceous sandstone overlain by low-permeability marls and shale. It has been characterized for oil exploration in a large number of wells as well as seismic lines, and a detailed geological model including depth and thicknesses of the target layers has been compiled within the MUSTANG project (Erlström et al., 2010, 2011). The experimental wells are located in the east part of the northern compartment where no oil was found. The roughly triangular-shaped northern compartment is bounded by pinch out of the target formation to the west and three sealing faults to the north, northeast and southwest, respectively, as shown in Fig. 1. At the location of the experimental wells the target formation is found at a depth from ground surface of about 1600 m and is dipping roughly 7.8°, with the direction of maximum dip roughly parallel to the southwest fault. A cross section showing the target layer and cap rock through the wells H-24, H-8, H-13, H-18 is available in Erlström et al. (2010).

The detailed geological model was simplified to a more practical model for the simulations of fluid flow and transport, shown schematically in Fig. 4, and which is still adequate for objectives of the study. For a simplified geometry and homogeneous geology, there is symmetry over the line of maximum dip. Hence, the flow and transport model was conceptualized as one symmetrical half of a dipping rectangular box aligned with the line of maximum dip. The volume of the model domain represented that of the closed North Heletz compartment (2.25×10^7 m^3) as calculated from the detailed geological model. Being one of two symmetrical halves, the total volume of the flow-model domain was the half that of the North Heletz compartment. Accordingly, the flow-model had a no-flow symmetry boundary running through the centres of both wells. It had a distance to second no-flow boundary in the y (strike) direction of 325 m based on the average distance from the wells to the southwest and northeast sealing faults (Figure 1). The distances from the abstraction well to the up-dip (2544 m) and down-dip (675 m) no-flow boundaries in the x-direction were determined so that the total volumes on each side of the well were in accordance with the detailed geological

model. These boundaries influenced the pressure build-up in the model, but otherwise had little effect on the simulated flow and transport of CO_2 and tracers, which occurred locally around the experiment wells as the experiment will use a relatively small volume of CO_2. Top and bottom boundaries were also no-flow.

The target formation has some embedded clay layers creating 3 possible sub-layers of sandstone. All these sub-horizons may or may not be present depending on the location of a well. In the flow model the three sub-horizons were lumped together to one single layer having a constant thickness equal to the effective sand thickness of 10.6m at the location of the experiment wells. The distance between the injection and abstraction well in the conceptual flow model was 50 m, while at the Heletz field site it will be slightly smaller.

Two discretizations of the model domain were used. Both grids used finer discretization around and between the wells and a coarser grid further away in the regions where CO_2 and tracers did not migrate. The wells were assumed to have effective radii of 0.20 m and were fully resolved by the grids. In the near-vertical z-direction the discretization was finer near the top of the model domain where the $scCO_2$ tended to accumulate under the cap rock ceiling as a buoyant pancake. The finer-discretized model used for the ECO2N simulations had 84 x 33 x 12 = 33264 grid blocks in x, y, z directions, respectively, and the coarser-discretized model used for the EOS7C simulations had 47 x 16 x 10 = 7520 grid blocks.

2.4 Model parameters

The amount of CO_2 that will be injected in the two-well dipole experiment at Heletz is roughly 1000 tons. The rate of injection may depend on the permeability of the formation, tolerance criteria for the used equipment and pressure build-up limit to ensure integrity of the cap rock. Here the rate of injection was taken as 5 tons/hour (which means 2.5 tons/hour in the symmetrical half model), which meant that the 1000 tons of CO_2 were injected in 8.33 days. The same rate was used for brine injection during the hydraulic tests. The fluid abstraction was modelled as a constant total rate of mass withdrawal of 5 ton/hour, where the fluid composition ($scCO_2$ / brine) was determined by the relative mobility of each fluid phase flowing to the well. The exact permeability (k), porosity (φ), residual $scCO_2$ (or gas) saturation (S_{gr}) and other parameters for the capillary pressure (P_c) and relative permeability (k_r) functions are not yet known at the location of the Heletz experiments. Awaiting results from hydraulic tests and core analyses, the permeability and porosity were taken somewhere in the middle of the range estimated from previous data from elsewhere in the target formation, such that $k = 50 \times 10^{-15}$ m^2 and $\varphi = 0.18$. In this simplified model, we assume that the permeability is isotropic even though there is evidence of horizontal layering within the target layer. Available parameters for the P_c and k_r functions were taken from data for Vosges-1 sandstone presented by Dana and Skoczylas (2002), which has similar porosity to the Heletz sandstone. These included the Brooks-Corey pore-size distribution index $\lambda = 0.762$, and the residual brine saturation $S_{wr} = 0.30$. The displacement pressure (P_d) for the Brooks-Corey P_c function was further scaled according to the method by Leverett (1941) to account for the difference in k between the Vosges-1 and Heletz sandstones yielding $P_d = 14.8$ kPa. The residual $scCO_2$ saturation (S_{gr}) was varied in the range 0.05 – 0.40 in different simulation scenarios, which was deemed a reasonable range judging a review of residual gas saturations presented by Holtz (2002).

2.5 Simulation scenarios

To test the sensitivity of the second hydraulic test to S_{gr} in the proposed test sequence, S_{gr} was varied between 0.09 and 0.30 using the ECO2N model on the higher resolution grid. These simulations were run for a long period of time after the CO_2 injection ended, and were also

used to illustrate how the state of the system changes during the test and how the state of residual $scCO_2$ saturation is detected so that the second hydraulic test can be performed at an appropriate time. Similar shorter simulations without the second hydraulic test but including the $scCO_2$-borne tracer were also performed using the EOS7C model. All these simulations are referred to as the base-case type scenario.

The variation in S_{gr} was deemed interesting also for evaluating how the dissolution behaviour could be captured by the test, because the variations in S_{gr} produced different spatial distributions of trapped $scCO_2$ and thereby also markedly different groundwater flow fields due to relative permeability effects. However, to further evaluate how the test could capture dissolution behaviour under a wider range of aquifer conditions and dissolution patterns, two additional types of scenarios were considered. First, the solubility of CO_2 used in the model was reduced by increasing its Henry's coefficient for equilibrium gas-water partitioning by a factor $10^{0.2}$ in favour of the $scCO_2$ phase, which is referred to as the reduced-solubility scenario. This scenario was also tested for a range of S_{gr} values. Generally, the solubility of CO_2 is a function of temperature, pressure, and fluid composition and the artificial reduction of CO_2 dissolution tests if the amount of dissolution can be inferred from the measured tracer and fluid compositions at the abstraction well. It can also be noted that an equilibrium partitioning model such as TOUGH2/EOS7C and ECO2N always overestimates the amount of dissolution that occurs and particularly when the discretization is coarse the overestimation can be large. The idea here, however, was not to exactly predict the dissolution that will take place in a real case, but to evaluate how well our proposed test sequence can detect that dissolution behaviour.

As a second scenario, we explored the idea that not all the residual water present in the sandstone (described by S_{wr}) may immediately become saturated with dissolved CO_2, and evaluated how this would be manifested in the output signals. This was done by replacing the residual water with solid rock in the model in such way that the flow field became exactly the same as it was with residual (immobile) water instead of rock, but in the rock case there was no uptake of dissolved CO_2 into the large volumes of residual water otherwise present in the model. This scenario is referred to as the no-dissolution-to-residual-water scenario and was also tested for a range of S_{gr} conditions. All simulation scenarios have been summarized in Table 1.

3. Results

3.1 Demonstration of the test sequence and the state of CO_2 during the experiment

Time zero in the test sequence is defined as the start of the reference hydraulic test (see also Fig. 2), and the times specified in the following result figures refer to this starting time. The reference hydraulic test (labelled "a" in Fig. 2) was modelled as 1 day abstraction only (well A), followed 1 day brine injection and 1 day recovery in well (I), with continuous abstraction in well (A). This was followed by injection of CO_2. Fig. 5 shows the spatial distribution of $scCO_2$ saturation (S_{scCO2}) in the vertical cross-section through the two wells for the base-case scenario simulated with the ECO2N model with $S_{gr} = 0.09$. During injection, the CO_2 migration was dominated by the injection pressure and directly after the injection (Fig. 5a), the $scCO_2$ had spread quite uniformly to a roughly radial distance of approximately 30 m around the injection well, with some effect of buoyancy driving the flow upward and together with the effect of abstraction also up dip, but CO_2 had not reached the abstraction well. Abstraction then continued to draw fluids to the up-dip well. CO_2 arrived at about 14 days after the start of the test (3 days after end of CO_2 injection), and by 71.3 days only a relatively small amount of mobile CO_2 remained under the cap rock ceiling (Fig. 5b).

When the mobile $scCO_2$ ceased to flow to the abstraction well from most of the vertical extent of the target layer, and instead only flowed as a thin pancake under the cap rock ceiling, there was a sharp change in rate of abstracted $scCO_2$. This is illustrated in Fig. 6, which shows the rate of CO_2 abstraction for the same simulation scenario. As can be seen in Fig. 6 at approximately 70 days after the start of injection, a sharp decline in $scCO_2$ outflow changed quite abruptly into a relatively constant, slow rate. The sharp decline was associated with disappearance of mobile CO_2 from the main part of the layer whereas the slow rate following it was associated with slow flow of the thin $scCO_2$ pancake under the ceiling. This type of abrupt change in $scCO_2$ outflow rate was also observed in the other simulation scenarios. Hence, it can provide a signal that mobile $scCO_2$ has disappeared from the main part of the formation and it is time to perform the second hydraulic test to measure residual $scCO_2$ saturation as further abstraction would now dissolve the residually trapped $scCO_2$.

Fig. 7 shows the mass of CO_2 in the aquifer as well as abstracted mass as functions of time for the base-case scenario with $S_{gr} = 0.09$. The amount of $scCO_2$ in the aquifer was related to the outflow pattern shown in Fig. 6, but was also affected by dissolution. At 133 days after the start of the simulation roughly 65% of the injected CO_2 had been abstracted either as supercritical phase or dissolved in brine. It can be noted that the simulated amount of dissolved CO_2 in the aquifer was relatively constant for a long period of time, and during this time the (cumulative) abstracted CO_2 increased almost linearly, indicating a constant rate of abstraction of dissolved CO_2, which also is in accordance with Figure 6. An estimation of the trapped $scCO_2$ in the aquifer is also shown in Fig. 7 under the assumption in the model that $scCO_2$ saturations below S_{gr} were trapped. When most of the mobile $scCO_2$ had been abstracted the trapped part dominated the $scCO_2$ present in the aquifer.

3.2 Hydraulic test

Fig. 8 shows the pressure (P) evolution with time for the base-case scenario with $S_{gr} = 0.09$ in the injection and abstraction wells, respectively. The reference hydraulic test produced the first peak in P at t = 2 days, which was followed by an increase in pressure due to the CO_2 injection (t = 3 – 11.3 days). Subsequently the pressure responses for 4 possible times of performing the second hydraulic test are shown. Following the proposed test sequence, the relevant time to perform the second test was at (roughly) 71 days after start of the experiment, shortly after the sharp change in abstraction rate of $scCO_2$ had been observed (as shown in Fig. 6). The rise in pressure (ΔP) produced by the second hydraulic test was then compared to the rise in pressure produced in the reference test (ΔP_{ref}) when no $scCO_2$ was present in the formation. The difference in pressure rise for both the injection well ($\Delta P_i - \Delta P_{i,\,ref}$) and the abstraction well ($\Delta P_a - \Delta P_{a,\,ref}$) are shown in Fig. 9 for different values of S_{gr}.

The simulations of the hydraulic test showed that the pressure signals in both the injection and abstraction wells were highly sensitive to the residual $scCO_2$ saturation. Because the abstraction well was continuously abstracting fluids at a constant rate, a positive but smaller pressure peak than in the injection well was observed (additional pressure felt from the injection well made it easier to abstract fluids). However, when S_{gr} became high ($S_{gr} = 0.30$) the additional pressure from the injection well during the test was hardly felt anymore such that $\Delta P_a = 0$, and $\Delta P_a - \Delta P_{a,\,ref} = -\Delta P_{a,\,ref}$. Therefore, for even higher S_{gr} values there would be no additional sensitivity to Sgr in abstraction well for this particular scenario. Nonetheless, it can be concluded that the pressure signal in the abstraction well provides an additional measurement of S_{gr} (to that obtained in the injection well) at least in the low S_{gr} range and for short enough distances between the two wells. It can also be noted that because all boundary conditions were closed and there was a net abstraction of fluids, the pressure in the system decreased with time.

3.3 Dissolved CO_2

The tracer test was aimed at providing information about the in-situ dissolution of CO_2. Fig. 10 shows a dissolved CO_2 budget for the base-case scenarios (4-8) including the dissolved CO_2 present in the formation together with the cumulative abstracted CO_2. The total dissolved CO_2 is given by the sum of dissolved CO_2 in the formation and cumulative abstracted dissolved CO_2. The increase with time of the total dissolved CO_2 is a measure of the effective (total) dissolution rate in the system. In Fig. 10 a constant effective dissolution rate (linear slope) has been fitted for total CO_2 dissolution during the time period 18 – 42 days when the amount of dissolved CO_2 in the formation started to stabilize and the total rate of dissolution became (roughly) constant. As can be seen in Fig. 10, the rise in cumulative abstracted dissolved CO_2 was also roughly linear for the same time period, which is related to constant rates of dissolved CO_2 abstraction. This general behaviour was observed for all scenarios, including the reduced-CO_2-solubility scenarios (9-13) and no-dissolution-to-residual-water scenarios (14-18) which were not included in Fig. 10 for brevity. In the scenarios with lower S_{gr} more dissolution was observed which was attributed partly to the fact that the $scCO_2$ can spread out more with less trapping and partly to the higher mobility of the aqueous phase in the regions with trapped $scCO_2$.

When all the different (EOS7C) scenarios were analysed together, a strong correlation was found between the effective total dissolution rate and the rate of dissolved CO_2 abstraction for the time period (18 -42 days) when the amount of dissolved CO_2 in the formation started to stabilize, as illustrated in Fig. 11. It should be noted that the 15 scenarios plotted in Fig. 11 span over a large range of different effective dissolution rates, which can attributed to the markedly different groundwater flow fields produced by the variation in the $scCO_2$ trapping parameter S_{gr} and the difference in CO_2 dissolution behaviour between the three types of scenarios. Yet, all scenarios showed a similar linear relationship between the rate of abstracted dissolved CO_2 and the total effective dissolution rate in the system. This result indicates that the rate of abstracted dissolved CO_2, as manifested in the proposed two-well test, is a robust measurement of effective total dissolution of CO_2 in the formation for a wide range of conditions.

3.4 Tracer test

The cumulative mass of tracer abstracted together with $scCO_2$ as a function of time is shown in Fig. 12. The effect of CO_2 dissolution on the tracer concentration in the $scCO_2$ phase was analysed by calculating the tracer enrichment which occurred as CO_2 dissolved while the tracer remained in the $scCO_2$ phase. The tracer enrichment was defined as the difference between the total tracer mass in the abstracted $scCO_2$ and the tracer mass that would have been abstracted if the tracer concentration had remained at its original value (baseline tracer abstraction). The baseline tracer abstraction was calculated from the mass of abstracted $scCO_2$ multiplied with the original mass fraction of tracer in the injected CO_2. At a relatively short time (in the order of 10 days) after $scCO_2$ breakthrough to the abstraction well (when the tracer became observable), the accumulation of both total abstracted tracer mass and enriched tracer mass appeared to become linear, and an effective tracer enrichment rate was calculated as the slope of the cumulative enriched tracer signal, also shown in Fig. 12. Similar linear behaviour was also found for all reduced-CO_2-solubility and no-dissolution-to-residual water scenarios, allowing calculation of tracer enrichment rates for all scenarios, except the base case with $S_{gr} = 0.40$ where no $scCO_2$ breakthrough was observed within the 45 day long simulation.

Next, the tracer enrichment rates were compared to the effective rate of CO_2 dissolution in the formation, again during the time period when the amount of dissolved CO_2 in the formation

had become roughly stable. When the effective dissolution rate of mobile $scCO_2$ was plotted against the tracer enrichment rate (Fig. 13), it was found that all dots fall roughly on the same curve, indicating that the dissolution rate of mobile $scCO_2$ could be described by the same correlation to the tracer enrichment rate for all the different scenarios. The mobile $scCO_2$ dissolution was calculated from the total $scCO_2$ dissolution and the known volumes of trapped and mobile $scCO_2$ under the assumption that mobile and immobile $scCO_2$ dissolved at the same rate, i.e. the dissolution rate of mobile $scCO_2$ was taken as the mobile $scCO_2$ fraction multiplied by the total $scCO_2$ dissolution rate.

Under this assumption, it can be concluded that the rate of tracer enrichment is both robust for a wide range of conditions in the formation and shows excellent correlation to the rate of mobile $scCO_2$ dissolution. It can further be concluded that the combination of the rate of abstracted dissolved CO_2 as a predictor for total CO_2 dissolution with the rate of tracer enrichment as a predictor for the dissolution rate of mobile $scCO_2$ allows analysis of the dissolution behaviour of both mobile and trapped $scCO_2$ in the system.

4. Discussion

The active abstraction of fluids from one of the two wells involved in the proposed two-well test allows monitoring of fluid flow and composition as well as certain control over the flow field. The results from the long, higher resolution ECO2N simulations (1-3) showed that the state of the system when it is appropriate to perform a second hydraulic test to measure residually trapped $scCO_2$ was readily detectable, and will be so in practice provided that the rate of abstracted $scCO_2$ can be continuously measured during a test. Generally, shortly after the $scCO_2$ had broken through to the abstraction well a flow pattern developed where the mobile $scCO_2$ flowed in the already established $scCO_2$ flow paths. When the $scCO_2$ no longer invaded new volumes of the aquifer, the amount of dissolved CO_2 present in the system also stabilized. This was deemed to be an important feature of the proposed two-well constant-abstraction type test, because the when the amount of dissolved CO_2 stabilized it became possible to analyse the effective rate of CO_2 dissolution in the formation using both the effluent dissolved CO_2 and negligible-solubility tracer (NST) signals.

The sensitivity of the hydraulic test to S_{gr} indicates that a hydraulic test is an effective tool for measurement of S_{gr} in the two-well test configuration as has also been shown previously for single-well tests to measure S_{gr} (Zhang et al., 2011). While the pressure signal in the abstraction well is sensitive to S_{gr} to the extent the pressure increase from the injection well is felt, more sensitivity to the local conditions around the abstraction well could be obtained if abstraction of fluids was stopped for some time before the second hydraulic test. The response would then be a negative peak in pressure mainly sensitive to the local mobility of fluids around the well. This variation of the test sequence was, however, not tested in this study. The generally decreasing pressure trend caused by net abstraction of fluids may have an impact on how the test should be implemented. In a small closed system such as the Heletz North compartment, the pumping rate and distance between the two wells need to be small enough to perform the full test sequence within acceptable changes in pressure.

The rate of abstracted dissolved CO_2 is strongly correlated to the total rate of dissolution provided that the amount of dissolved CO_2 in the formation is stable. However, the tracer enrichment in the $scCO_2$ is strongly correlated to the dissolution rate of mobile $scCO_2$ irrespective of whether the amount of dissolved CO_2 is stable or not. Consequently, negligible-solubility tracer techniques can be applied to measure dissolution of mobile $scCO_2$ also under other conditions than the two-well continuous abstraction test where the amount of dissolved CO_2 in the formation stabilizes. For example, this technique can also be used to

measure the dissolution of CO_2 from a plume of $scCO_2$ over the long term, at any scale from a small-scale research experiment to a commercial or demonstration-scale CO_2 injection project. Here the measurement of the dissolution rate of the plume could be used to verify if a convective mixing process enhancing the dissolution of CO_2 has commenced. It has been proposed that density-driven convective mixing processes can greatly enhance the CO_2 dissolution to brine (e.g. Lindeberg and Bergmo, 2003), particularly in high-permeability storage formations where the onset of this process will be fast (e.g. Riaz et al., 2006). A direct measurement of the CO_2 dissolution rate in-situ would be of great value to verify theoretical analyses and models of enhanced CO_2 dissolution by convective mixing. The present tracer technique provides such a possibility provided that the $scCO_2$ plume can be sampled through a sampling and monitoring borehole.

5. Concluding remarks

A two-well test sequence to measure both residual and dissolution trapping of CO_2 in a geological storage formation was presented. It was shown that the pressure signals in both wells during a hydraulic test can be used to measure the residual $scCO_2$ saturation in the formation, and that the correct timing for the hydraulic test can be readily determined from a continuous measurement of the rate of abstracted $scCO_2$.

CO_2 dissolution and tracer transport in the system was analysed for a range of markedly different groundwater flow fields produced by variation in the $scCO_2$ trapping parameter S_{gr} as well as 3 different types of CO_2 dissolution behaviour manifested in a base-case, reduced-CO_2-solubility, and no-dissolution-to-residual-water scenario. The different simulation scenarios produced a wide range of effective CO_2 dissolution rates in the system. It was shown that the total rate of CO_2 dissolution in the system had a strong correlation to the rate of abstracted dissolved CO_2 over this wide range of conditions.

It was further shown that a tracer of negligible aqueous solubility injected with the $scCO_2$ could provide direct information about the dissolution of mobile $scCO_2$. When $scCO_2$ was abstracted from the second well the tracer concentration had increased due to dissolution of CO_2 into brine. The rate of tracer enrichment showed excellent correlation with the rate of mobile $scCO_2$ dissolution over the same wide range of dissolution conditions tested. It can be concluded that the combination of the measurements of abstracted dissolved CO_2 and tracer allow the possibility to determine the dissolution rates of both mobile and trapped $scCO_2$ and thereby constitute a promising tool for detailed characterization of the CO_2 dissolution process in-situ.

The correlation of the total CO_2 dissolution rate to the dissolved CO_2 abstraction rate relies on the ability of the two-well continuous-abstraction test to establish a stable flow regime where the amount of dissolved CO_2 in the formation stabilizes. However, the negligible-solubility tracer enrichment in the $scCO_2$ is not dependent on the amount of dissolved CO_2 in the formation, and can be applied to measure the dissolution of mobile $scCO_2$ also in other applications, such as for verification of enhanced CO_2 dissolution by convective mixing processes in long-term monitoring of $scCO_2$ plumes.

Acknowledgements

The research leading to these results has received funding from the Swedish Research Council for Environment, Agricultural Sciences and Spatial Planning (FORMAS), project n° 214-2008-1032, and from the European Community's 7th Framework Programme FP7/2007-2013, under grant agreement n° 227286. We also thank two anonymous reviewers for their insightful comments.

References

Akervoll, I., Zweigel, P., Lindeberg, E., 2006. CO_2 storage in open dipping aquifers. Proceed. GHGT-8, Trondheim.

Brooks, R.H., Corey, A.T., 1964. Hydraulic properties of porous media. Hydrology paper 3, Colorado State University, Fort Collins, Colorado.

Burdine, N.T., 1953. Relative permeability calculations from pore size distribution data. Trans. Am. Inst. Min. Met. Eng., 198, 71-78.

Dana, E., Skoczylas, F., 2002. Experimental study of two-phase flow in three sandstones. II. Capillary pressure curve measurement and relative permeability pore space capillary models. International Journal of Multiphase Flow 28 (11), 1965-1981.

Doughty, C., Freifeld, B.M., Trautz, R.C., 2008. Site characterization for CO_2 geologic storage and vice versa - the Frio brine pilot, Texas, USA as a case study. Environ. Geol., 54(8) 1635-1656.

Du, Y., Guan, L., 2005. Interwell tracer tests: lesson learned from past field studies. Soc. Petrol. Engineers, SPE paper 93140.

Erlström, M., Silva, O., de Vries, L.M., Shtivelman, V., Gendler, M., Goldberg I., Scadeanu D., Sperber, C.M., 2010. Deliverable D022: 3D structures of test sites. MUSTANG, EU-FP7 proj. no. 227286, Public report avail. at: www.co2mustang.eu

Erlström, M., Roetting, T., Sperber, C.M., Shtivelman, V., Scadeanu D., 2011. Deliverable D023: Report on property values and parameters, related uncertainties. MUSTANG, EU-FP7 proj. no. 227286, Public report avail. at: www.co2mustang.eu

Fagerlund, F., Niemi, A., Illangasekare, T.H., 2008. Modeling of NAPL migration in heterogeneous saturated media: Effects of hysteresis and fluid immobility in constitutive relations. Water Resources Research 44, W03409, doi:10.1029/2007WR005974.

Fagerlund, F., Illangasekare, T.H., Niemi, A., 2007a. Nonaqueous-phase liquid infiltration and immobilization in heterogeneous media: 1. Experimental methods and two-layered reference case. Vadose Zone J. 6: 471-482. doi:10.2136/vzj2006.0171.

Fagerlund, F., Illangasekare, T.H., Niemi, A., 2007b. Nonaqueous-phase liquid infiltration and immobilization in heterogeneous media: 2. Application to stochastically heterogeneous formations. Vadose Zone J. 6: 483-495. doi:10.2136/vzj2006.0172.

Hesse, M.A., Orr Jr., F.M., Tchelepi, H.A., 2009. Gravity currents with residual trapping. Energy Proceedia, 1, 3275-3281.

Holtz, M.H. 2002. Residual gas saturation to aquifer influx: A calculation method for 3-D computer reservoir model construction. Soc. Petrol. Engineers, SPE paper 75502.

IPCC, 2005. IPCC Special Report on Carbon Dioxide Capture and Storage. Prepared by Working Group III of the Intergovernmental Panel on Climate Change. Metz, B., O. Davidson, H.C. de Coninck, M. Loos, and L.A. Meyer, (eds.) Cambridge Univ. Press.

Jin, M., Delshad, M., Dwarakanath, V., McKinney, D. C., Pope, G. A., Sepehrnoori, K., Tilburg, C. E., Jackson, R. E., 1995. Partitioning tracer test for detection, estimation, and remediation performance assessment of subsurface nonaqueous phase liquids. Water Resour. Res. 31, 1201–1211.

Kneafsey, T., Pruess, K., 2010. Laboratory flow experiments for visualizing carbon dioxide-induced, density-driven brine convection. Transp. Porous Media, 82(1), 123-139.

Krevor, S., Pini, R., Li, B., Benson, S., 2011. Capillary heterogeneity trapping of CO_2 in a sandstone rock at reservoir conditions, Geophysical Research Letters, 38, L15401.

Land, C.S., 1968. Calculation of imbibition relative permeability for two- and three phase flow from rock properties. Soc. Petrol. Eng. J. Trans. Am. Inst. Min. Metall. Pet. Eng. 243:149-156.

Lengler, U., De Lucia, M., Kühn, M., 2010. The impact of heterogeneity on the distribution of CO_2: Numerical simulation of CO_2 storage at Ketzin, International Journal of Greenhouse Gas Control, 4(6), 1016-1025, doi:10.1016/j.ijggc.2010.07.004.

Leverett, M.C., 1941. Capillary behavior in porous solids. Trans. AIME, 142, 152-169.

Lindeberg, E., Bergmo,P., 2003: The long-term fate of CO_2 injected into an aquifer. Proceedings of the 6th International Conference on Greenhouse Gas Technology.

Mariner, P.E., Jin, M.Q., Studer, J.E., Pope, G.A., 1999. The first vadose zone partitioning interwell tracer test for nonaqueous phase liquid and water residual. Environ. Sci. Technol. 33(16), 2825–2828.

Nelson, N.T., Oostrom, M., Wietsma, T.W., Brusseau, M.L., 1999. Partitioning tracer method for the in situ measurement of DNAPL saturation: influence of heterogeneity and sampling method. Environ. Sci. Technol. 33 (22), 4046–4053.

Neufeld, J.A., Hesse, M., Riaz, A., Hallworth, M., Tchelepi, H., Huppert, H.E., 2010. Convective dissolution of carbon dioxide in saline aquifers. Geophys. Res. Letters 37, L22404.

Oldenburg, C., Moridis, G., Spycher, N., Pruess, K., 2004. EOS7C Version 1.0: TOUGH2 module for carbon dioxide or nitrogen in natural gas (methane) reservoirs. Report LBNL-56589, Lawrence Berkeley National Laboratory, Berkeley, California.

Pau, G., Bell, J., Pruess, K., Almgren, A., Lijewski, M., Zhang, K., 2010. High-resolution simulation and characterization of density-driven flow in CO_2 storage in saline aquifers. Adv. Wat. Resour. 33(4), 443–455.

Polak, S., Cinar, Y., Holt, T., Torsæter, O., 2010. An experimental investigation of the balance between capillary, viscous and gravitational forces during CO_2 injection into saline aquifers. Energy Proceedia, GHGT-10.

Pruess, K., Oldenburg, C., Moridis, G., 1999. TOUGH2 User's Guide, Version 2.0. Report LBNL-43134, Lawrence Berkeley National Laboratory, Berkeley, California.

Pruess, K., 2005. ECO2N: A TOUGH2 fluid property module for mixtures of water, NaCl, and CO_2. Report LBNL-57952, Lawrence Berkeley National Laboratory, Berkeley, California.

Pruess, K., Freifield, B., Kennedy, M., Oldenburg, C., Phelps, T.J., and van Soest, M.C., 2005. Use of gas phase tracers for monitoring CO_2 injection at the Frio Test Site: presented at the National Energy Technology Laboratory Fourth Annual Conference on Carbon Capture and Sequestration, Alexandria, Virginia, May 2-5, 2005. GCCC Digital Publ. Series 05-04r, 1-17.

Qi, R., LaForce, T.C., Blunt, M.J. 2009. Design of carbon dioxide storage in aquifers. Intl. J. Greenhouse Gas Control, 3, 195-205.

Riaz, A., Hesse, M., Tchelepi, H.A., Orr Jr., F.M., 2006. Onset of convection in a gravitationally unstable diffusive boundary layer in porous media. J. Fluid Mechanics, Vol. 548, 87-111.

Sinha, R., Asakawa, K., Pope, G.A., Sepehrnoori, K., 2004. Simulation of natural and partitioning interwell tracers to calculate saturation swept volumes in oil reservoirs. Soc. Petrol. Engineers, SPE paper 89458.

Suekane, T., Nobuso, T. , Hirai, S., Kiyota. M., 2008. Geological storage of carbon dioxide by residual gas and dissolution trapping. Intl. J. Greenhouse Gas Control, 2(1), 58-64.

Tang, J.S., 2005. Extended Brigham model for residual oil saturation measurement by partitioning tracer tests. Soc. Petrol. Engineers, SPE paper 84874.

Wen, W.-Y., Muccitelli, J. A., 1979. Thermodynamics of Some Perfluorocarbon Gases in Water. J. Solution Chemistry, 8 (3), 225-246.

Wuerdemann, H., Moeller, F., Kuehn, M., Heidug, W., Christensen, N.P., Borm, G., Schilling, F.R., and the CO2Sink Group, 2010. CO2SINK - From site characterisation and

risk assessment to monitoring and verification: One year of operational experience with the field laboratory for CO_2 storage at Ketzin, Germany. Int. J. Greenhouse Gas Control, 4(6) 938-951.

Zhang, Y., Freifeld, B., Finsterle, S., Leahy, M., Ennis-King, J., Paterson, L., et al. (2011). Single-well experimental design for studying residual trapping of supercritical carbon dioxide. Int. J. Greenhouse Gas Control, 5, 88-98.

Figures and Tables

Table 1. Summary of simulation scenarios.

Scenario number	Scenario type	Code	Grid resolution	S_{gr}
1 - 3	Base case	ECO2N	High	0.09, 0.2, 0.3
4 - 8	Base case	EOS7C	Low	0.05, 0.1, 0.2, 0.3, 0.4
9 - 13	Reduced CO_2 solubility	EOS7C	Low	0.05, 0.1, 0.2, 0.3, 0.4
14 - 18	No dissolution to res. water	EOS7C	Low	0.05, 0.1, 0.2, 0.3, 0.4

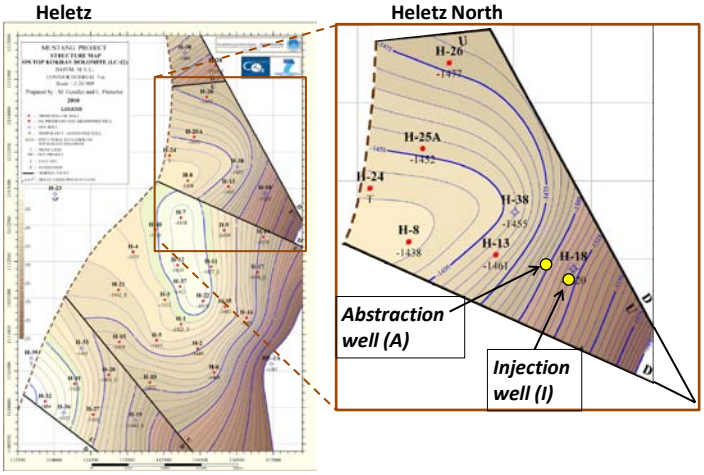

Fig. 1. Map of the target formation for CO_2 field injection experiments at Heletz, Israel, (based on the structure map by Gendler and Fleischer, in Erlström et al., 2010).

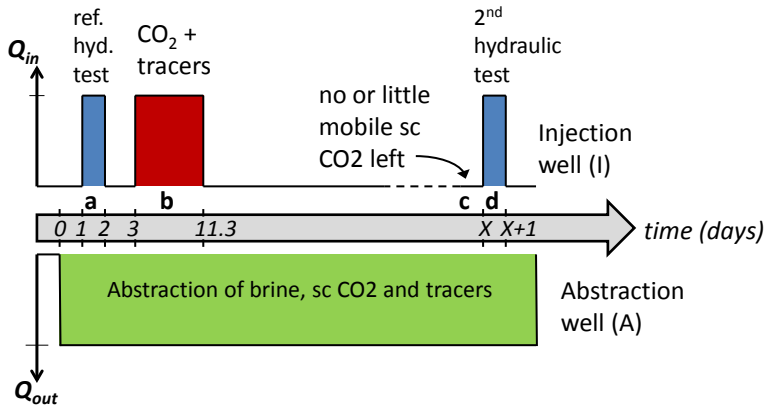

Fig. 2. Proposed dipole experiment injection-abstraction sequence. Time zero is the start of the reference hydraulic test.

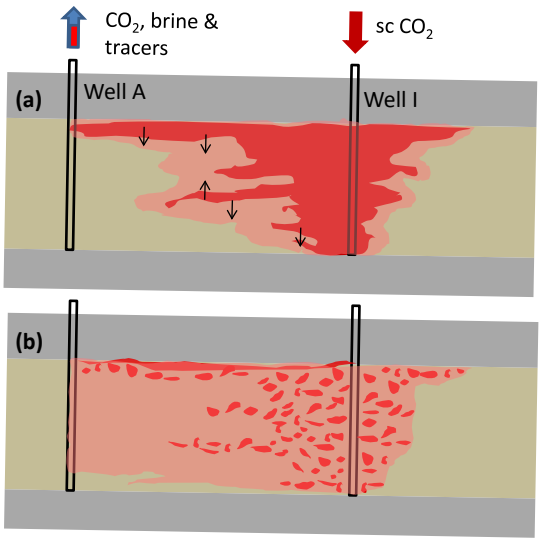

Fig. 3. Dipole CO_2 injection experiment at breakthrough to abstraction well (a) and at residual state of $scCO_2$ (b).

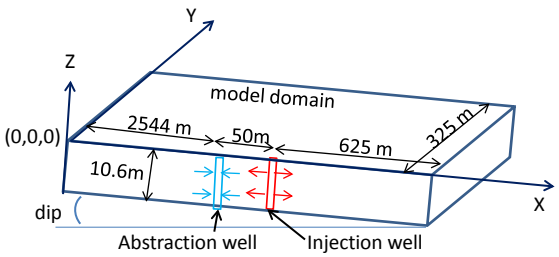

Fig. 4. Schematic drawing of the dipping, symmetrical-half 3D model domain.

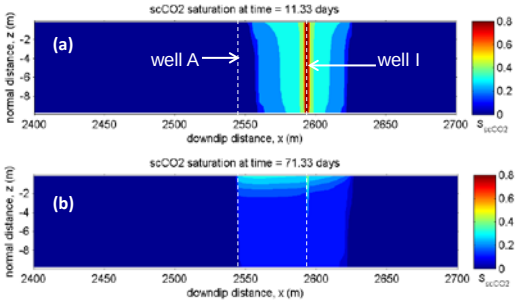

Fig. 5. Spatial distribution of $scCO_2$ in the vertical cross-section through the two wells directly after injection (11.33 days) and at a time when little mobile $scCO_2$ remains in the formation (71.33 days) in the base-case, S_{gr} = 0.09 simulation. Injection and abstraction wells are marked I and A, respectively.

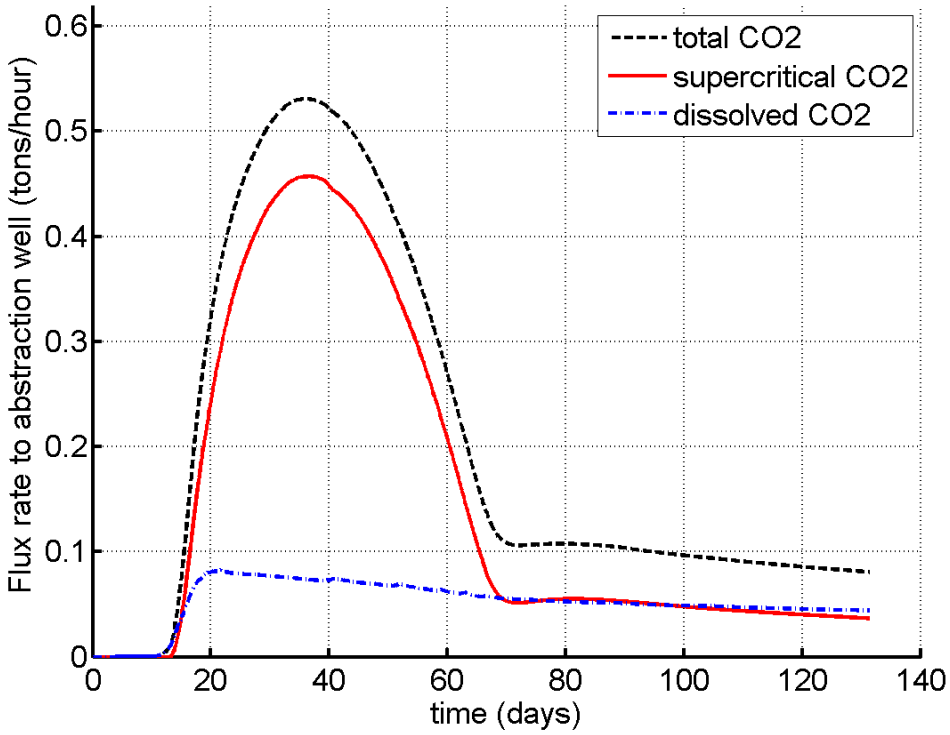

Fig. 6. Flux of CO_2 to the abstraction well for the base-case scenario simulated with the fine-grid ECO2N model. Time zero is the start of the hydraulic reference test and the CO_2 injection is from t = 3 – 11.3 days (see also Fig. 2).

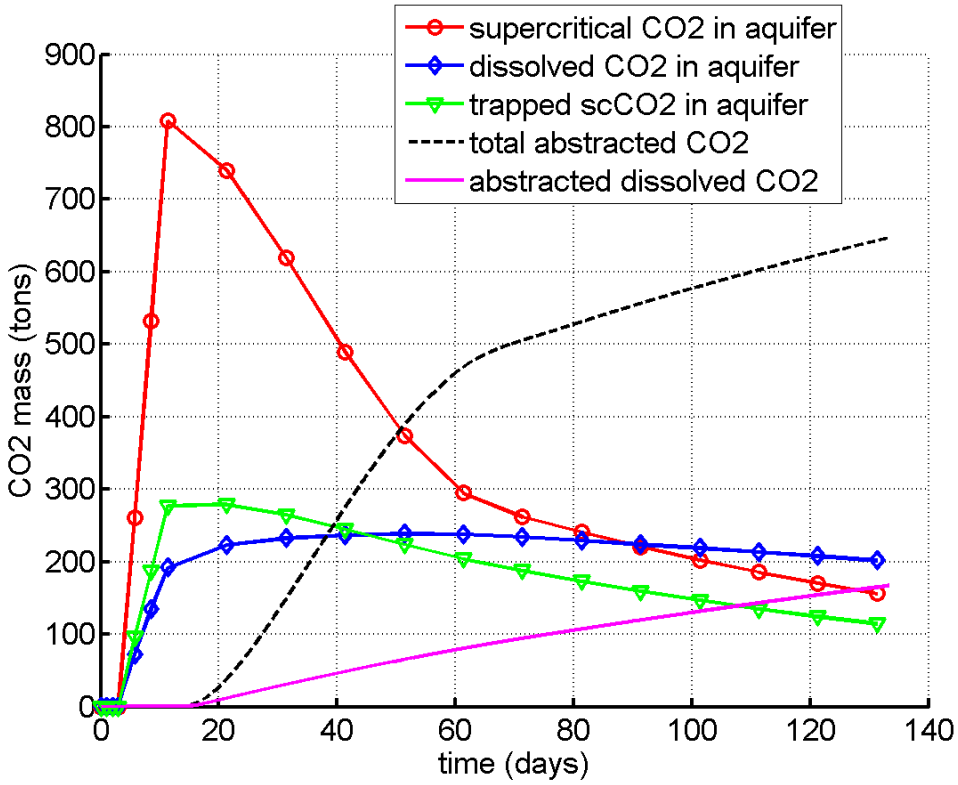

Fig. 7. Distribution of CO_2 with time for the base-case scenario with S_{gr} = 0.09.

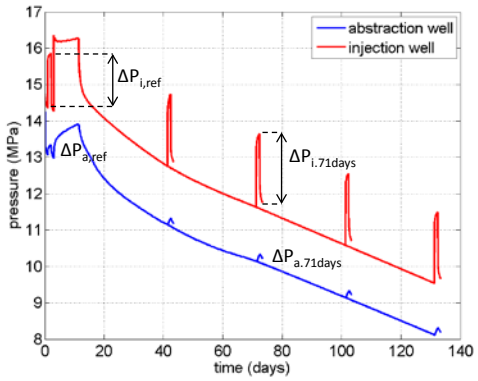

Fig. 8. Pressure in the wells as a function of time for the base-case scenario with S_{gr} = 0.09. ΔP is the change in pressure in response to hydraulic tests at different times.

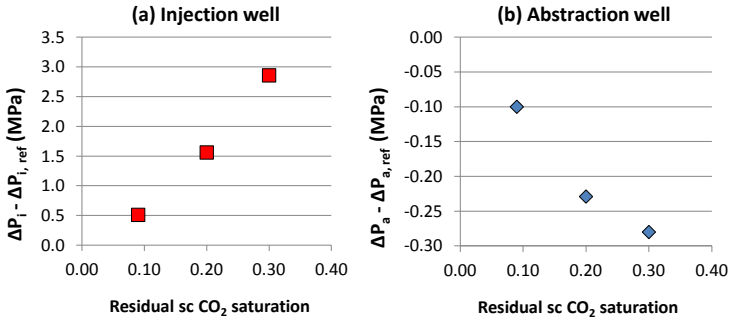

Fig. 9. Difference in pressure response between the reference hydraulic test and the second test at residual $scCO_2$ conditions (ΔP - ΔP_{ref}) for simulations using different residual $scCO_2$ values; (a) in the injection well, and (b) in the abstraction well.

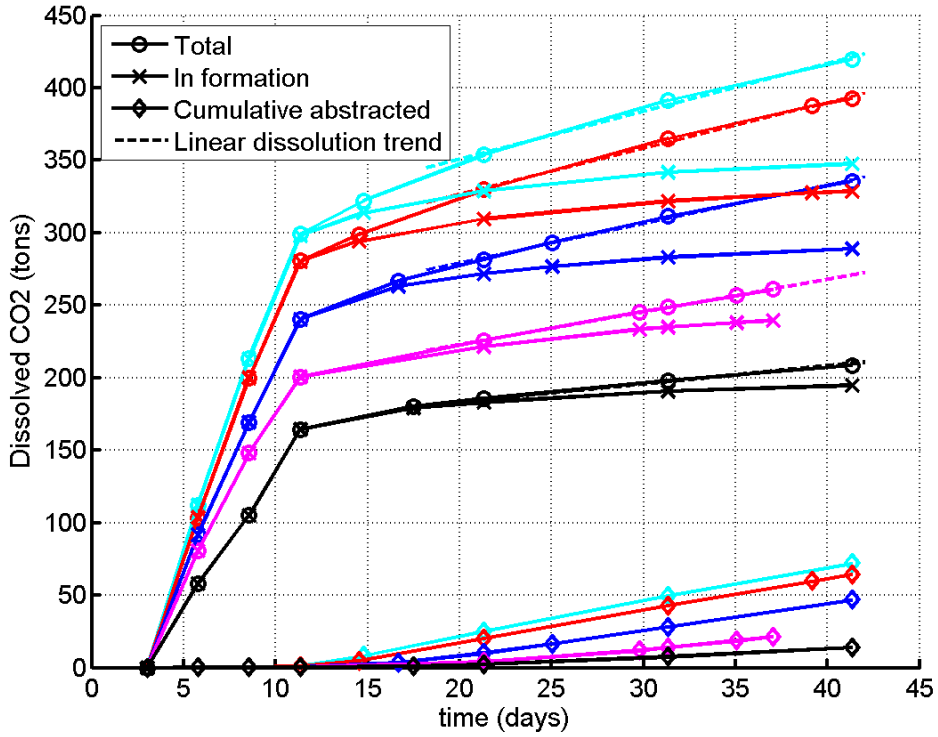

Fig. 10. Dissolved CO_2 budget for the base-case scenario. The results for S_{gr} = 0.05, 0.10, 0.20, 0.30, 0.40 are indicated by the colours: cyan, red, blue, magenta and black, respectively. The slopes of the fitted dashed lines (linear dissolution trends) show effective CO_2 dissolution rates during the time period 18 – 42 days.

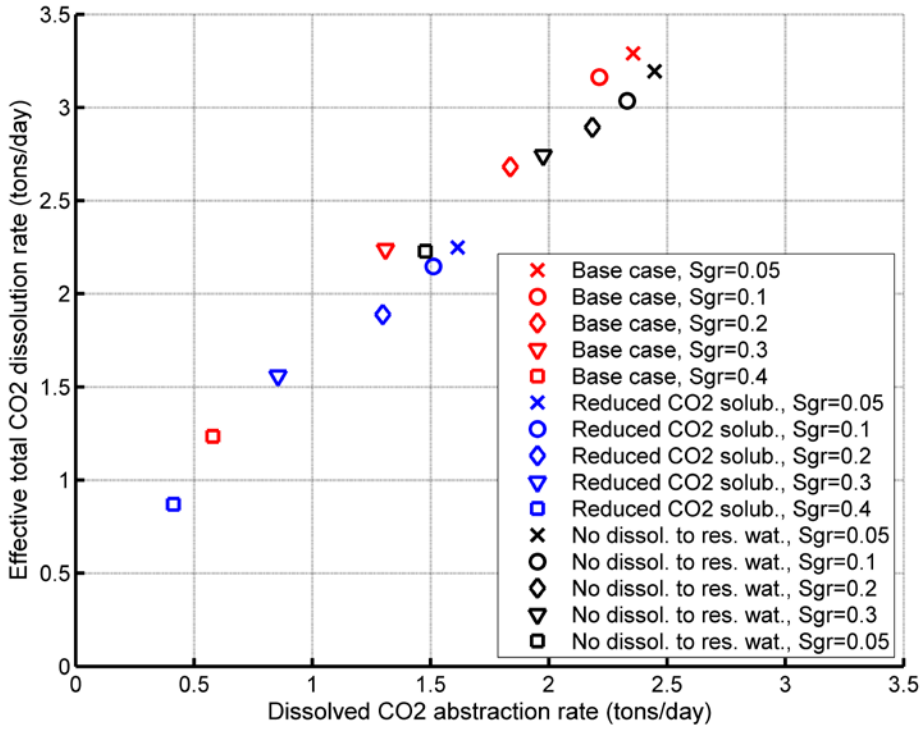

Fig. 11. Effective total CO_2 dissolution rate as a function of dissolved CO_2 abstraction rate for the time period 18 - 42 days after start of experiment.

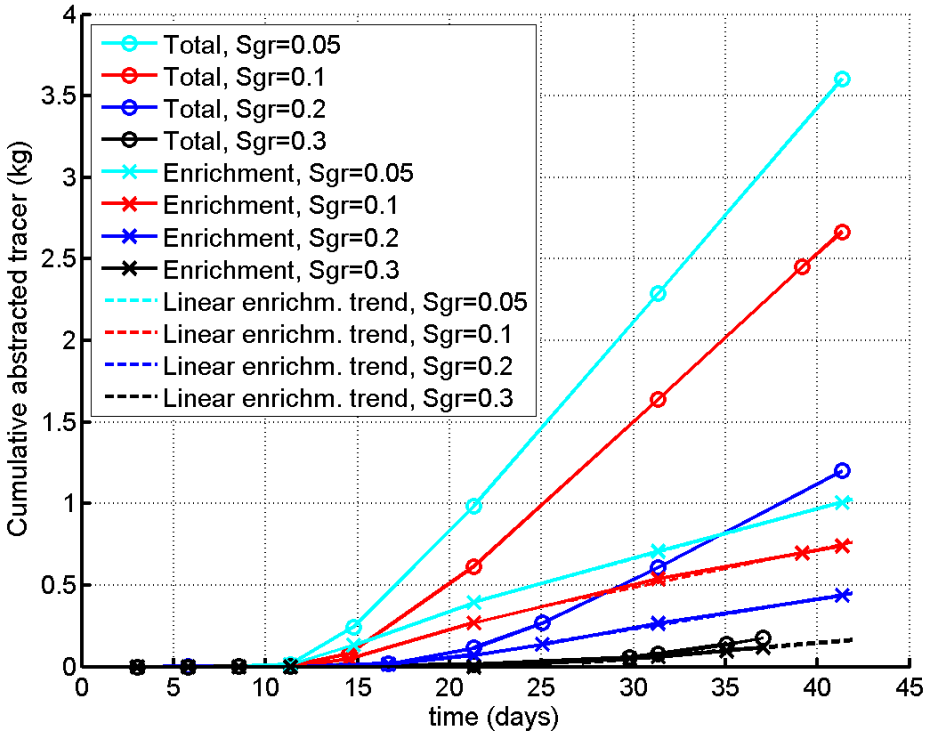

Fig. 12. Pumped out tracer mass in $scCO_2$ for the base-case scenario. Tracer enrichment has been calculated as the difference between the (total) tracer mass in the abstracted $scCO_2$ and the expected (baseline) tracer mass that would have been abstracted if the tracer concentration

had remained at its original value. The slopes of the dashed fitted lines (linear enrichment trends) show the effective enrichment rates during the time period 25 – 42 days.

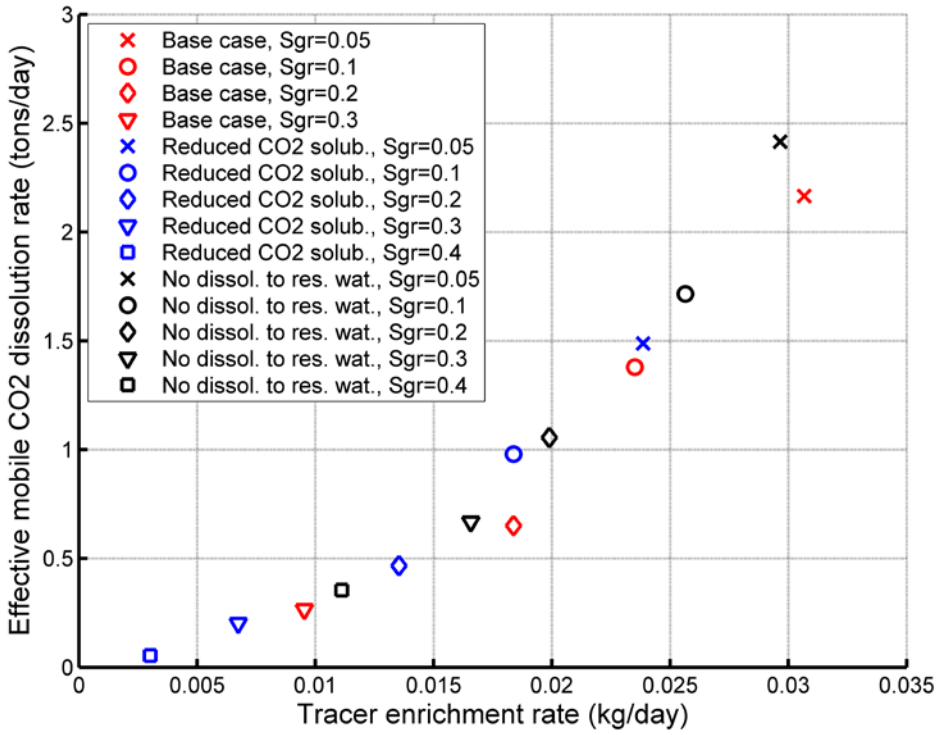

Fig. 13. Effective dissolution rate of mobile CO_2 as a function of tracer enrichment rate in abstracted scCO_2 in the time period 18 - 42 days after start of the experiment simulation.